

Influence of combined Al_2O_3 - SiO_2 filler on thermal and dielectric properties of barium zinc borate glass microcomposites for barrier ribs of plasma display panels

Mousumi Das, Shiv Prakash Singh, Karan Pal,
Suchika Jena & Basudeb Karmakar*

Glass Technology Laboratory, Glass Division,
Central Glass and Ceramic Research Institute (Council of Scientific and Industrial Research),
196. Raja S.C. Mullick Road, Kolkata 700 032, India

Abstract

The co-effects of Al_2O_3 - SiO_2 filler to an extent of 25 wt. % on thermal (softening point and coefficient of thermal expansion) and dielectric constant of lead free BaO - ZnO - B_2O_3 - SiO_2 - Li_2O - Na_2O (BZBSLN) glasses have been explored with a view to use as barrier ribs of plasma display panels (PDPs). The interaction of fillers with glass occurred during firing (570°C) has also been investigated by XRD, SEM micrograph and FTIR spectroscopy analyses. The fillers have been found to be partially dissolved in the glass at the firing temperature leaving some unreacted residual filler which result in ceramic-glass microcomposites. All the properties are found to follow the same experimental and theoretical trends, and regulate by the covalent character as well as the optical basicity of microcomposites. Addition of combined filler found to be yielded the required properties and meeting the criteria for barrier rib application.

Keywords: Powders-solid state reaction, glass, composites, thermal properties, dielectric properties

*For correspondence (basudebk@cgcricri.res.in)

Introduction

Plasma display panels (PDPs) are characterized by larger screen sizes¹⁻⁵ (over 100 inches), wide viewing angle, more accurate image reproduction with better colour accuracy, contrast and brightness, superior ability to display moving images without motion artifacts and better pixel reliability over liquid crystal displays LCDs. Barrier ribs which lie between the front and rear glass substrates form the partition between the phosphor cavities to prevent optical cross-talk (i.e., color from one pixel leaking into an adjacent pixel). Lead containing borosilicate glasses were mainly used for the barrier ribs of PDP because of their low softening temperature (less than 580⁰C), low coefficient of thermal expansion, CTE (less than 83 x 10⁻⁷/K) and low dielectric constant, DC (less than 15) with respect to use of PD200 glass as PDP substrate. Presently various glass powders such as PbO-ZnO-B₂O₃ and PbO-ZnO-SiO₂ is being used for barrier ribs which contain huge amount (60-80%) of lead oxide (PbO)⁶. Recently, lead free glass systems are of immense interest for its application on barrier ribs due to the hazardous effects of lead on health and environmental concerns.

Lead free BaO-ZnO-B₂O₃-SiO₂ (BZBS) and BaO-ZnO-B₂O₃ (BZB) glass systems have been reported as alternatives⁷⁻¹¹ for barrier ribs of PDP. Chong et. al.¹²⁻¹³ has reported the BaO-ZnO-B₂O₃-P₂O₅ glass system for the same. In this work, we have selected a lead-free multicomponent barium zinc borate, BaO-ZnO-B₂O₃-SiO₂-Li₂O-Na₂O (BZBSLN) glass system for barrier ribs and investigated its ability to form microcomposites with various types of fillers. Above all, barium zinc borate system is not hazardous¹⁴. Crystalline ceramic fillers Al₂O₃ and amorphous SiO₂ are added to form a

ceramic particulate-glass microcomposite to modify its softening point, CTE and DC. As we aware, this work has not been reported previously.

In view of above, in this study we report the combined effect the Al_2O_3 (crystalline, $\alpha\text{-Al}_2\text{O}_3$) and SiO_2 (amorphous) fillers to an extent of 25 wt% on the softening point (T_s), coefficient of thermal expansion (CTE) and dielectric constant (ϵ_r) of BaO-ZnO-B₂O₃-SiO₂-Li₂O-Na₂O glass. The glass-filler interaction which occurs at the sintering temperature has also been investigated by XRD, SEM images and FTIR spectral analyses. The thermal and dielectric properties of glass microcomposites have been analyzed with regard to their covalent character and optical basicities.

Experimental Procedure

Preparation of glass and microcomposite

The batch of the BaO-ZnO-B₂O₃-SiO₂-Li₂O-Na₂O (BZBSLN) glass was prepared by using the high purity raw materials such as BaO (GR, 99%, Merck), ZnO (GR, 99%, Loba Chemie), H₃BO₃ (GR, 99.5%, Loba Chemie), SiO₂ (Quartz), Li₂CO₃ (GR, 99%, Loba Chemie) and Na₂CO₃ (GR, 99%, Loba Chemie). About 500 g glass was melted in a platinum crucible in an electrically heated raising hearth furnace at 1150°C for 2h in air with intermittent stirring. The molten glass was quenched by casting into an iron plate. The quenched glass was initially crushed in a stainless steel mortar and then pulverized in a planetary mono mill (Retzch, Model PM100) using zirconia jar and ball to obtain final glass powders of 10.1 μm size (d_{50}).

The pulverized BZBSLN glass powders were mixed well in isopropanol medium with appropriate amount of amorphous microsilica, SiO₂ (Pooja Enterprises, 99.5 %, d_{50}

= 1.5 μm) and alpha alumina, Al_2O_3 (Alcoa, 99.9 %, $d_{50} = 2.0 \mu\text{m}$) fillers in an agate mortar. All the powders were then granulated using 2 wt% aqueous solution of polyvinyl alcohol (PVA) followed by pressing uniaxially into disk or cylindrical shape of desired sizes under a pressure of 500 kgf/cm^2 and then dried. It was sintered at 570°C for 2h in air for measurement of CTE, T_g , ϵ_r , XRD, SEM photomicrograph and FTIR spectra. The compositions of composites are enlisted in Table 1.

Characterization technique

The softening point (T_s) of the dried disk was measured by a glass softening point system (Harrop/Labino, Model SP-3A) with an accuracy of $\pm 1^\circ\text{C}$. The instrument was previously calibrated with a NBS (National Bureau of Standards, USA) standard glass of known softening point. The CTE of the sintered microcomposite cylinders were measured with an accuracy of $\pm 1\%$ using a horizontal-loading dilatometer (Netzsch, Model 402C) after calibration with a standard alumina supplied with the instrument by the manufacturer. The CTE in the temperature range 50-350°C is reported here. The dielectric constant was measured with an accuracy of $\pm 1\%$ at a frequency of 1MHz using a LCR meter (Hioki, Model 3532-50 LCR Hitester) at 25°C. The instrument was calibrated previously by a Suprasil-W silica glass ($\epsilon_r = 3.8$). XRD data were recorded using XPERTPRO diffractometer with Ni-filtered and anchor scan parameter wavelength 1.54060 Å ($\text{CuK}\alpha$) at 25°C with power of 40 kV and 30 mA at the scan speed 10°/min. The SEM images of the samples were carried out in LEO S430i instrument at 15 kV. The samples were examined after Au coating on the surface to pass the electron beam through it. FTIR spectra were recorded by dispersing the sintered glass and microcomposite powders in KBr with a Perkin-Elmer FTIR spectrometer (Model 1615) at a resolution of

$\pm 2 \text{ cm}^{-1}$ after 16 scans. It was calibrated with a polystyrene film supplied by the instrument manufacturer. Particle size analyses of powders were carried out using a Malvern Instrument (Model Mastersizer 2000).

Glass properties such as Littleton softening point (T_{Lt}) and CTE were theoretically calculated (predicted) using SciGlass (Glass Properties Information System, Version 6.7) software following the Priven-2000 method¹⁵⁻¹⁸ and dielectric constant by the method of Kharjuzov and Zorin¹⁸.

Results and Discussion

Particle size distribution

It is well known that the degree of glass-filler interaction (powders-solid state reaction) is largely depended on their particle size and its distribution. Smaller the particle sizes of the glass or filler greater the extent of interaction. Thus, the particle size distribution of BZBSLN glass powder, Al_2O_3 and SiO_2 fillers are measured and shown in Fig.1. It is seen that only SiO_2 and BZBSLN glass powders exhibit a bimodal particle size distribution whereas Al_2O_3 exhibits unimodal particle size distribution. The median particle sizes (d_{50}) of BZBSLN glass powder, Al_2O_3 and SiO_2 fillers are found to be 10.1, 2.0 and 1.5 μm respectively.

XRD analysis

As the reaction of fillers (Al_2O_3 and SiO_2) with glass during firing at 570°C is the fundamental to the formation of filler-glass microcomposites, thus they have been examined by XRD analysis. The variation of XRD patterns with added Al_2O_3 - SiO_2 filler content is shown in Fig. 2. BZBSLN glass is X-ray amorphous (Fig.2, curve a). Since the

added SiO₂ filler is amorphous (see Fig.2, curve f) so there is no XRD peak of SiO₂ whereas Al₂O₃ filler is corundum, alpha alumina (see Fig.2, curve g), so the microcomposite MC1 containing highest Al₂O₃ exhibits well developed XRD pattern of corundum Al₂O₃ (JCPDS card file No.: 43-1484) with diminished amorphous character (see curve b). With gradual decrease in Al₂O₃ content and increase in SiO₂ content, the characteristic peaks of corundum Al₂O₃ decrease and amorphous character gradually increases. XRD pattern also indicates that the filler has partially dissolved in glass during sintering at 570°C leaving behind some residual filler in the glass matrix which exhibit their characteristic peaks. This observation correlates well with those of FTIR spectral study as discussed later (see section 3.3). Thus, it is clear from XRD analysis that combined Al₂O₃-SiO₂ filler containing microcomposites are of crystal (ceramic)-in-amorphous characteristics.

Microstructural analysis

The microstructure of the composites, sintered at 570°C with SiO₂ and Al₂O₃ fillers was characterized by SEM photomicrographs. The sintered samples were prepared by grinding and polishing followed by etching in 1% aqueous solution of HF for 60 s. The dried samples were examined after Au coating on the surface to pass the electron beam through it. The fact that the fillers has partially dissolved in the glass matrix during sintering is evidenced by SEM images of the microcomposites as shown in Fig. 3 (a) and (b) of samples MC1 and MC3 respectively. They also show the distribution of fillers in the microcomposites after sintering. It is seen from Fig. 3 (a) of microcomposite MC1 which contains 20% Al₂O₃ and 5% SiO₂ fillers that Al₂O₃ is partially dissolved in the glass whereas a large number of small irregular spherical particles of SiO₂ found to be

embedded in the glassy matrix. It is seen that the degree of solubility of Al_2O_3 is higher than that of SiO_2 . The glassy matrix is distinctly visible here. However, the picture is entirely different in Fig. 3 (b) of composite MC3 which contains 10% Al_2O_3 and 15% SiO_2 fillers. Here it is seen that Al_2O_3 dissolves almost completely and SiO_2 fillers remain relatively undissolved. Some pores are found in the SEM micrographs which indicate that the density of the sintered microcomposites would be less than that of glass

FTIR spectra analysis

The FTIR spectra of Al_2O_3 - SiO_2 containing microcomposites are depicted in Fig.4. Their IR band positions along with nature and assignments are also provided in Table 2. The BZBSLN glass exhibits four distinct bands around 1377, 969, 700 and 577 cm^{-1} , which are attributed to asymmetric stretching vibration of B-O-B bond of the trigonal $[\text{BO}_3]$ units, symmetric stretching vibration of B-O-B bond of the tetragonal $[\text{BO}_4]$ units, bending vibration of B-O-B linkages of the borate glass networks¹⁸⁻²⁰ and bending vibration of B-O-Si linkages respectively.

The SiO_2 filler exhibits three intense bands around 1115, 815 and 477 cm^{-1} which are attributed to asymmetric stretching vibration of Si-O-Si bond, symmetric stretching vibrations of O-Si-O bond and bending vibration of Si-O-Si bond of $[\text{SiO}_4]$ tetrahedral respectively¹⁸. It is seen from Fig. 3 that with increasing SiO_2 filler in the microcomposites MC1 to MC4 all these three bands gradually become more intense along with the intensity decrease and changes of the shape of all the three bands of the BZBSLN glass. These observations have been more clearly enlisted in Table 2. The bands at around 1239 and 939 cm^{-1} are attributed to asymmetric vibration of B-O-Si

bond¹⁹. This fact clearly indicates the distinct interaction of BZBSLN glass with SiO₂ filler.

The Al₂O₃ (corundum) filler, on the other hand, exhibits doublet bands at 645 and 615 cm⁻¹ which are attributed to asymmetric and symmetric stretching vibrations of Al-O-Al bond of octahedral [AlO₆]²¹⁻²³ units of Al₂O₃ molecules. Whereas its remaining band at 462 cm⁻¹ is due to bending vibration of Al-O-Al bond. It is also seen that initially in microcomposite MC1 having 20 wt% Al₂O₃ the band at 700 cm⁻¹ of BZBSLN glass undergoes pronounced change and takes almost the similar shape of Al₂O₃ (compare curves b and g). However, with decreasing Al₂O₃ filler in the microcomposites MC2 to MC4, this band undergoes a gradual change and the bands related to Al₂O₃ filler at 646 and 615 cm⁻¹ gradually become less intense (see Fig.4, curve b-e). In addition the 969 cm⁻¹ band undergoes changes with formations of medium intense band at around 939 cm⁻¹ which are due to asymmetric vibration of B-O-Si respectively. This is clearly shown in Table 2. All the facts clearly indicate the distinct interaction of BZBSLN glass with Al₂O₃ and SiO₂ fillers. It is seen from that the nature of the spectra of microcomposites due to combined Al₂O₃-SiO₂ addition gradually becomes closer to the individual filler at its respective highest content but has the mixed nature at their intermediate content. It further indicates that both the fillers have partially dissolved in the glass leaving behind residual fillers in the resultant microcomposites. This is analogous to the observation of XRD analysis as discussed earlier.

Softening point

The softening point (T_s) gradually increase as the SiO₂ content in the combined Al₂O₃-SiO₂ filler increases from 5 to 20 wt%. Similar increasing trends are observed in

the theoretically predicted Littleton softening point (T_{Ll}). This fact is depicted in Fig. 5. The close correlation between the experimental and theoretically calculated (predicted) softening point clearly indicates that these properties are additive in nature with respect to the constituting chemical components. This is because of the fact that theoretical calculation of the T_{Ll} is based on additive mathematical formula¹⁵⁻¹⁷ as shown below.

$$P = \sum_{i=1}^N g_{i,P} m_i n_i \sum_{i=1}^N m_i n_i \quad (1)$$

where P is the property being calculated, i is the index of the oxide, N is the number of types of oxides forming the glass microcomposite in question, m_i is a molar fraction of the i^{th} oxide, n_i is the number of atoms in the formula of the i^{th} oxide and $g_{i,P}$ is a partial coefficient for the i^{th} oxide.

A similar increasing trend of glass transition temperature with increasing SiO₂ content has been demonstrated by Vernacotola and Shelby²⁵⁻²⁶ for potassium niobium silicate glasses. To explain this fact, some properties of added Al₂O₃ and SiO₂ fillers are provided in Table 3. The increase of T_g is due to high melting points of Al₂O₃ (2100°C) and SiO₂ (1723°C) fillers. It is also seen from Fig. 5 that SiO₂ filler has greater effect on softening point as compared to Al₂O₃ filler. This is due to higher electronegativity of Si (1.8) than Al (1.5) (see Table 3) which results in higher covalent character as well as lower optical basicity of the ultimate microcomposites with increasing SiO₂ content.

The extent of covalent bonding character of the resultant microcomposites can be calculated approximately using the formula²⁷.

$$\text{Covalent character (\%)} = \exp [-0.25 (\Delta\chi)^2] \times 100 \quad (2)$$

where $\Delta\chi$ is the electronegativity of the composite, that is, the electronegativity difference ($\chi_A - \chi_C$) of the anions and the cations. The average electronegativity of the anions (χ_A) or cations (χ_C) can be evaluated by the following simple additive relation²⁸.

$$\chi_A \text{ or } \chi_C = \sum N_i \chi_i / \sum N_i \quad (3)$$

where N_i and χ_i are the number of individual constituent atom per mole and its electronegativity, respectively.

Optical basicity²⁹ of microcomposites can be calculated by using the formula

$$A_c = X_1 A_1 + X_2 A_2 + \dots + X_n A_n \quad (4)$$

or

$$A_c = X_1/\gamma_1 + X_2/\gamma_2 + \dots + X_n/\gamma_n \quad (5)$$

where A_1, A_2, \dots, A_n are the basicities assigned to individual oxide and $\gamma_1, \gamma_2, \dots, \gamma_n$ are the corresponding basicity moderating parameters. X_1, X_2, \dots, X_n are the equivalent fractions based on the amount of oxygen each oxide contributes to the overall glass stoichiometry.

The variation of experimental softening point, T_s of microcomposites MC1-MC4 as a function of its covalent character as well as optical basicity is shown in Figs.5 and 6 respectively. It is seen that T_s increase with increase in covalent character whereas the same decreases with increase of optical basicity of the microcomposites. This is due to the inverse relation of the covalent character with the optical basicity. This has been depicted in Fig. 7. Thus, there exists a direct relation between the T_s with the covalent character and an inverse relation with the optical basicity of the microcomposites and seems to be guided by these fundamental properties of microcomposites.

Coefficient of thermal expansion

Comparison of variation of experimental and theoretically predicted coefficient of thermal expansion (CTE) as a function of added Al_2O_3 or SiO_2 filler content is shown in Fig.8. The CTE of composites gradually decreases as SiO_2 filler content increases from 5 to 20 wt%. Vernacotola and Shelby²⁵⁻²⁶ have also found a similar decreasing trend of CTE with increasing SiO_2 content in potassium niobium silicate glasses. It is seen from Table 3 that SiO_2 filler has very low CTE ($5.5 \times 10^{-7}/\text{K}$) as compared to the glass ($82 \times 10^{-7}/\text{K}$). The resultant CTE of the composite, therefore, decreases gradually. This fact also supports the additive character (see Eq. 1) of CTE of the composites with respect to their chemical components as seen earlier in the case of T_s .

The above fact can also be well understood from the decrease in CTE with increase in covalent character (see Fig. 10) associated with the decrease of optical basicity of microcomposites which results in strengthening of connectivity of the network of composites. The behaviour of CTE of the microcomposites with optical basicity is shown in Fig.11. Thus, CTE bears an inverse relation and a direct relation with the covalent character and optical basicity of the microcomposites respectively.

Dielectric constant

Dielectric constant (ϵ_r) of the microcomposites has been calculated by using the following formula³⁰

$$\epsilon_r = cd/(0.0885 A) \quad (6)$$

where c , d and A are capacitance in pico Farad (pF), thickness of glass or microcomposite (in cm) and area of the dielectric (in cm^2) respectively.

The comparison of variation of experimental and theoretically predicted dielectric constant as a function of added Al_2O_3 or SiO_2 fillers is shown in Fig. 12. The theoretical predictions are lower than the experimentally obtained values. It is seen that the dielectric constant of the composites gradually decreases with increase in SiO_2 filler content. Both the trends correlate very well. It is seen from Table 3 that the dielectric constant of SiO_2 filler is 3.8 which is lower than that of the glass (9.3) whereas the dielectric constant of Al_2O_3 filler is nearly same (9-10) to that of the glass. Thus, the resultant dielectric constant of combined Al_2O_3 - SiO_2 filler added composite gradually decreases with increasing SiO_2 content or decreasing Al_2O_3 content. This once again supports in favour of the additive nature of dielectric constant like other properties such as T_s and CTE as described earlier, that is, there is a direct relationship between the property values of fillers and the resultant microcomposites. The variation of dielectric constant of composites MC1-MC4 as a function of their covalent character is already shown in Fig.10. It is also seen that the dielectric constant of the composites decreases with increase in their covalent character whereas it decreases with decrease of optical basicity (see Fig.11). Thus, dielectric constant bears an inverse relation and a direct relation with the covalent character and optical basicity of the microcomposites respectively and seems to be regulated by them.

Conclusions

In this effort to unfold a lead-free environmental-friendly alternative microcomposites for the barrier ribs of plasma display panels, the co-effect of Al_2O_3 - SiO_2 ceramic fillers to an extent of 25 wt% on the softening point, coefficient of thermal

expansion and dielectric properties of multicomponent BaO-ZnO-B₂O₃-SiO₂-Li₂O-Na₂O (BZBSLN) glass has been investigated. Based on qualitative XRD, SEM micrograph and FTIR spectral analyses, both the fillers investigated are found to be partially dissolved in the glass at the sintering temperature (570°C), and thus the specimen successfully formed ceramic filler particulate-reinforced glass matrix microcomposites with a strong interfacial bonding. The softening point, T_s has been found to be increased whereas coefficient of thermal expansion (CTE) and dielectric constant, ϵ_r decreased with increasing SiO₂ content. The close correlation of theoretical predictions and experimental values strongly advocates the additive nature of the physical properties with respect to the chemical constituents of the composites. Covalent character and optical basicity are two guiding parameters to predict the nature of microcomposites. The chemical behavior of the microcomposites have been analysed in terms of two fundamental properties of chemical bond such as covalent character and optical basicity. It is seen that there exists an inverse relation between them. The increase and decrease of thermal and dielectric properties correlate well with the covalent character and optical basicity of the resultant microcomposites. The co-addition of Al₂O₃-SiO₂ filler to BZBSLN is found to be more effective in consideration of the desired properties of barrier ribs for PDPs.

Acknowledgements

This research has been supported in part by the NMITLI programme of CSIR, New Delhi. The authors gratefully thank Dr. H. S. Maiti, Director of the institute for his keen interest and kind permission to publish this paper. They also acknowledge the Ceramic Membrane, XRD and Electron Microscope Division of this institute for carrying

out the particle size measurement, XRD and SEM photomicrograph experiments respectively.

References

- 1 Mattox D M & Robinsion J H, *J Am Ceram Soc*, 80 (1997) 1189.
- 2 Jean J H, Lin S C & Yang S L, *J Appl Phys*, 34 (1995) L422.
- 3 Hwang G H, Jeon H J & Kim Y S, *J Am Ceram Soc*, 85 (2002) 2956.
- 4 Fukushima N, Oshita H & Mito T, *US pat.* 6417123B1, 2002.
- 5 Jung B H, Lee D K, Sohn S H & Kim H S, *J Am Ceram Soc*, 86 (2002) 1202.
- 6 Hwang G H, Kim W Y, Jeon H J & Kim Y S, *J Am Ceram Soc*, 85 (2006) 2961.
- 7 Kim S G, Park J S, An J S, Hong K S, Shin H & Kim H, *J Am Ceram Soc*, 89 (2006) 902.
- 8 Shin H, Kim S G, Park J S, An J S, Hong K S & Kim H, *J Am Ceram Soc*, 89 (2006) 3258.
- 9 Sreeram A N, Quinn R L & Prabhu A N, *US pat.* 6140767, 2000.
- 10 Okunaga, Kiyoyuki, Kitamura, Yoshirou, Gotou, Tatsuya, Ohji, Masahiko, Hadano, Kazuo, *US pat.* 6737373, 2004.
- 11 Kim S G, Shin H, Park J -S, Hong K S & Kim H, *J Electroceram*, 15 (2005) 129.
- 12 Chong E, Hwang S, Shin H & Kim H, *Int. J. Thermophys.*, (in press).
- 13 Chong E, Hwang S, Sung W & Kim H, *Int J Appl Ceram Technol*, (in press).
- 14 Yawa C L, *Chemical Properties Handbook: Physical, Thermodynamic, Environmental, Transport, Safety and Health Related Properties for Organic and Inorganic Chemicals*, (McGraw-Hill Book Co., New York), 1999, 613-615.

- 15 Priven A I, *Glass Tehnol*, 45 (2004) 244.
- 16 Priven A I, *Glass Phys and chem*, 24 (1998) 67.
- 17 Priven A I & Mazunin O V, *Glass Technol*, 44 (2003) 156.
- 18 SciGlass (Glass Properties Information System), Version 6.7
- 19 Fuxi G, *Optical and Spectroscopic Properties of Glass*, (Springer-Verlag, Berlin), 1992, 18-61.
- 20 Kamitsos E I, Karakassides A M & Chryssikos D G, *J Phys Chem*, 91 (1987) 1073.
- 21 Motke S G, Yowale S P & Yawale S S, *Bull Mater Sci*, 25 (2002) 75.
- 22 Burdick V L & Day D E, *J Am Ceram Soc*, 50 (1997) 97.
- 23 Kolesova V A, *The Structure of Glass*, Vol.2, (Translated from Russian, Consultants Bureau, New york,), 1960, 177.
- 24 Stubičan V & Roy R, *Am Mineral*, 46 (1961) 32.
- 25 Vernacotola D E, *Key Engg Mater*, 94-95 (1994) 379.
- 26 Vernacotola D E & Shelby J E, *Phys Chem Glasses*, 35 (1994) 153.
- 27 Pauling L, *The Nature of the Chemical Bond*, 3rd edn. (Cornell University Press, New York), 1960, 34-75.
- 28 Karmakar B, *J Solid State Chem*, 178 (2005) 2663.
- 29 Duffy J A & Ingram M D, *Optical Properties of Glass*, ed. By Uhlmann D R & Kreidl N J, (The American Ceramic Society, Inc, Westerville, USA), 1991, 159-184.
- 30 Dakin T K, Insulating Materials-General Properties, in *Standard Handbook for Electrical Engineers*, ed. By Fink D G & Beaty H W, 13th edn., (McGraw Hill Inc, New York,), 1993, 4-117 -130.

Figure caption

Fig. 1 - Particle size distribution of BZBSLN glass, SiO₂ and Al₂O₃ filler powders

Fig. 2 - Variation of XRD patterns with Al₂O₃ and SiO₂ filler content: (a) glass, G, (b) MC1, (c) MC2, (d) MC3, and (e) MC4 (for composition see Table 1). XRD patterns of added fillers (f) SiO₂ and (g) Al₂O₃ fillers are also provided for comparison

Fig. 3 - SEM images of microcomposites (a) MC1 and (b) MC3 (for composition see Table 1) showing the distribution of SiO₂ and Al₂O₃ fillers in the glass matrix

Fig. 4 - FTIR spectra of (a) glass, G, (b) MC1, (c) MC2, (d) MC3 and (e) MC4. (For composition see Table 1). Spectra of added (f) SiO₂ and (g) Al₂O₃ fillers are also given for comparison

Fig. 5 - Comparison of variation of experimental and theoretically calculated softening point, as a function of added Al₂O₃ or SiO₂ filler of microcomposites MC1-MC4 (for composition see Table 1)

Fig. 6 - Variation of experimental softening point, T_s of microcomposites MC1-MC4 (for composition see Table 1) as a function of their covalent character

Fig. 7 - Variation of experimental softening point, T_s of microcomposites MC1-MC4 (for composition see Table 1) as a function of their optical basicity

Fig. 8 - Inverse relationship of covalent character of microcomposites MC1-MC4 (for composition see Table 1) as a function of their optical basicity

Fig. 9 - Comparison of variation of experimental and theoretically calculated coefficient of thermal expansion (CTE) as a function of added Al_2O_3 or SiO_2 filler of microcomposites MC1-MC4 (for composition see Table 1)

Fig. 10 - Variation of coefficient of thermal expansion (CTE) and dielectric constant (ϵ_r) of microcomposites MC1-MC4 (for composition see Table 1) as a function of their covalent character

Fig. 11 - Variation of coefficient of thermal expansion (CTE) and dielectric constant (ϵ_r) of microcomposites MC1-MC4 (for composition see Table 1) as a function of their optical basicities

Fig. 12 - Comparison of variation of experimentally and theoretically calculated dielectric constant (ϵ_r) as a function of added Al_2O_3 or SiO_2 filler of microcomposites MC1-MC4 (for composition see Table 1)

Table 1 - Composition of microcomposites derived from BaO-ZnO-B₂O₃-
SiO₂-Li₂O-Na₂O (BZBSLN) glass

Sample identity	Composition (wt%)		
	BZBSLN Glass	Added Al ₂ O ₃ filler	Added SiO ₂ filler
G	100	-	-
MC1	75	20	5
MC2	75	15	10
MC3	75	10	15
MC4	75	5	20

Table 2 - IR band position in glass, microcomposites, SiO₂ and Al₂O₃ fillers along with assignment

G	Sample identity / Band position (cm ⁻¹)				SiO ₂ filler	Al ₂ O ₃ filler	Band assignment
	MC1	MC2	MC3	MC4			
1377(s,b)	1377(s,b)	1377(s,b)	1377(s,b)	1377(s,b)			B-O-B(as-s)
1231(sh)	1239(s,b)	1231(s,b)	1208(s,b)	1208(s,b)			B-O-Si(as-s)
	1069(s,b)	1108(s)	1115(s)	1115(s)	1115(s)		Si-O-Si(as-s)
969(s,b)	939(sh)	939(sh)	939(m)	939(m)			B-O-B(as-s), B-O-Si(as-s)
			808(m)	808(m)	815(s)		O-Si-O(s-s)
700(s)							B-O-B(b-v)
		685(sh)		685(s)			B-O-B(b-v)
	646(s)	654(s)	646(s)			646(s)	Al-O-Al(as-s)
	608(s)	608(s)	608(s)	608(s)		615(s)	Al-O-Al(s-s)
577(s,b)							B-O-Si(b-v)
					477(s)		Si-O-Si(b-v)
	462(s)	462(s)	462(s)	469(s)		462(s)	Al-O-Al(b-v)

s = strong, b = broad, w = weak, sh = shoulder, m = medium

s-s = symmetric stretching vibration, as-s = asymmetric stretching vibration

b-v = bending vibration

Table 3 - Some properties of added SiO ₂ and Al ₂ O ₃ fillers					
Filler	Crystallinity	Melting point (°C)	CTE (x10 ⁻⁷ /K)	Dielectric constant, ε _r	Si or Al Electronegativity, χ
SiO ₂	Amorphous	1723	5.5	3.8	1.8
Al ₂ O ₃	Crystalline (alpha-alumina)	2100	70-80	9-10	1.5

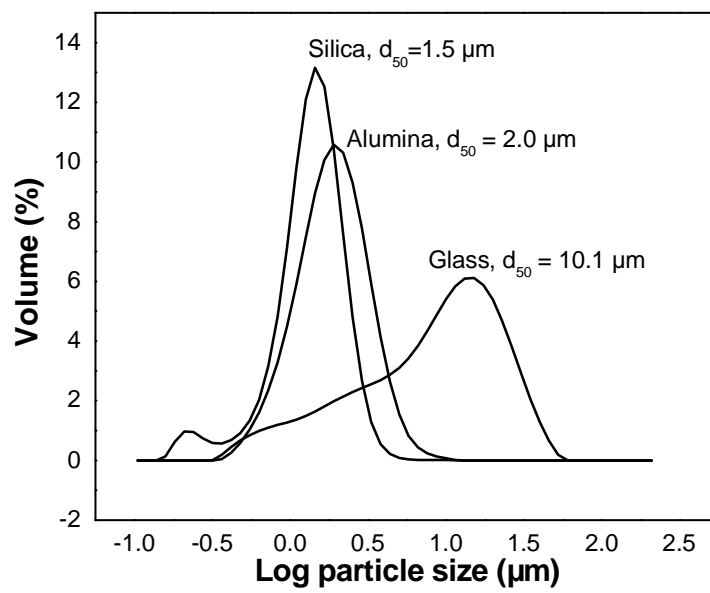


Fig. 1 - Particle size distribution of BZBSLN glass, SiO₂ and Al₂O₃ filler powders

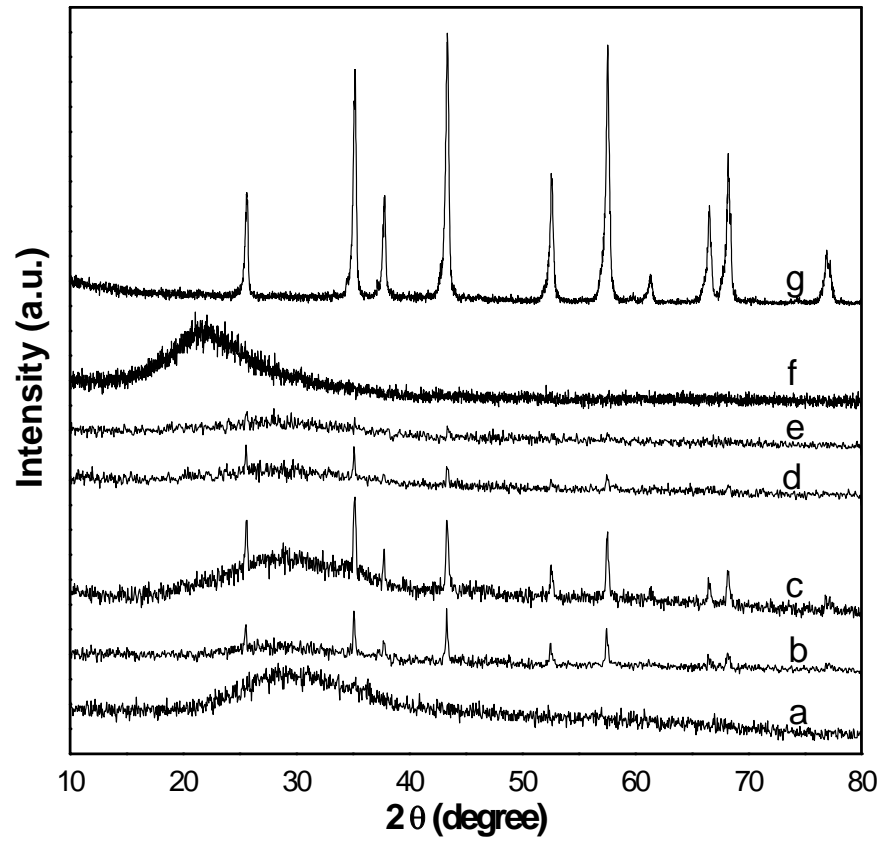


Fig. 2 - Variation of XRD patterns with Al_2O_3 and SiO_2 filler content: (a) glass, G, (b) MC1, (c) MC2, (d) MC3, and (e) MC4 (for composition see Table 1). XRD patterns of added fillers (f) SiO_2 and (g) Al_2O_3 fillers are also provided for comparison

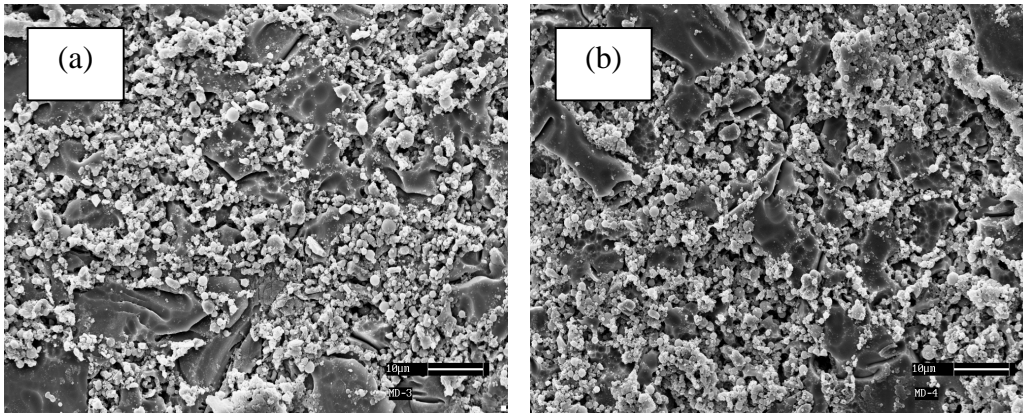


Fig. 3 - SEM images of microcomposites (a) MC1 and (b) MC3 (for composition see Table 1) showing the distribution of SiO_2 and Al_2O_3 fillers in the glass matrix

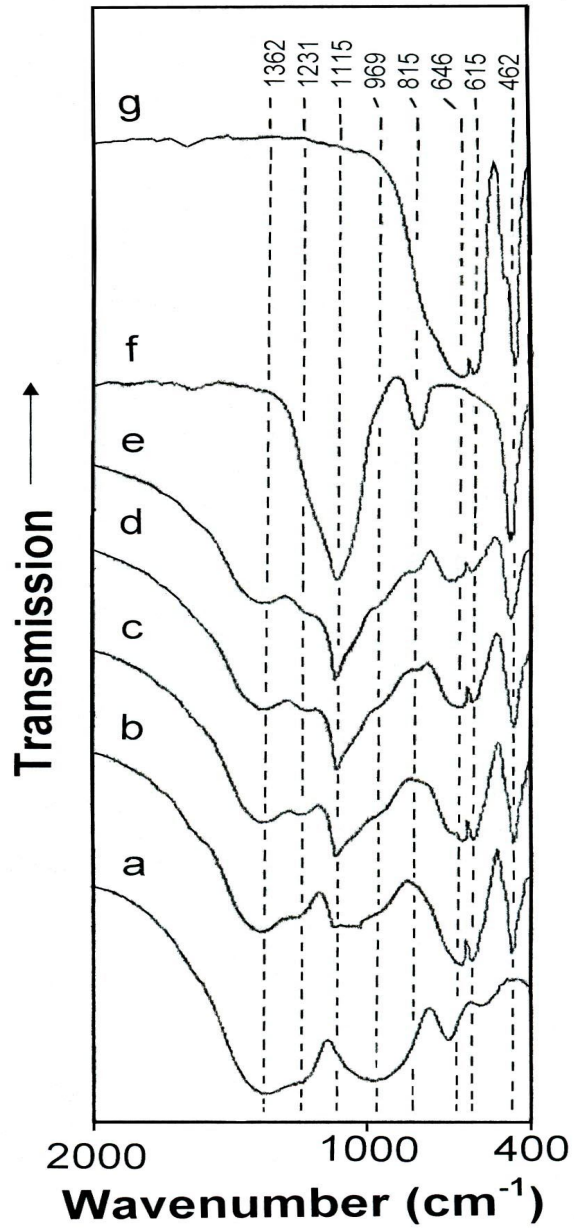


Fig. 4 - FTIR spectra of (a) glass, G, (b) MC1, (c) MC2, (d) MC3 and (e) MC4. (For composition see Table 1). Spectra of added (f) SiO₂ and (g) Al₂O₃ fillers are also given for comparison

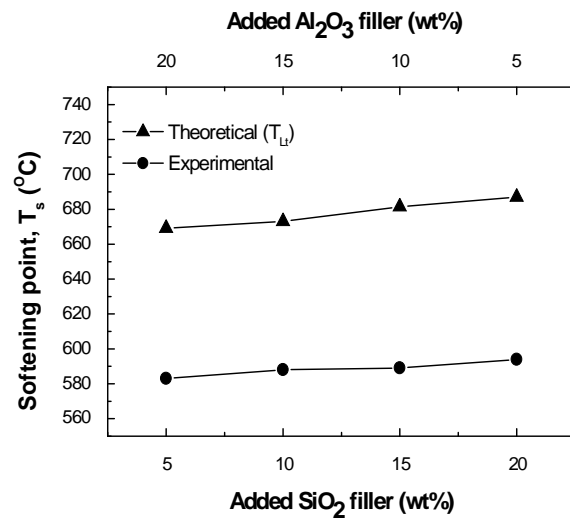


Fig. 5 - Comparison of variation of experimental and theoretically calculated softening points, as a function of added Al_2O_3 or SiO_2 filler of microcomposites MC1-MC4 (for composition see Table 1)

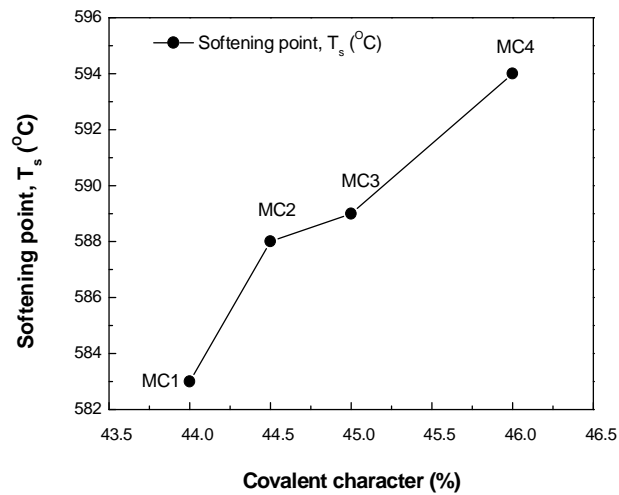


Fig. 6 - Variation of experimental softening point, T_s of microcomposites MC1-MC4 (for composition see Table 1) as a function of its covalent character

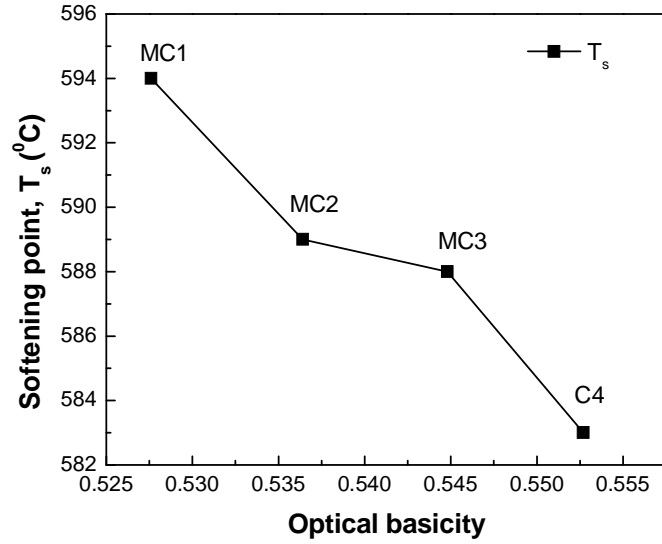


Fig. 7 - Variation of experimental softening point, T_s of microcomposites MC1-MC4 (for composition see Table 1) as a function of their optical basicity

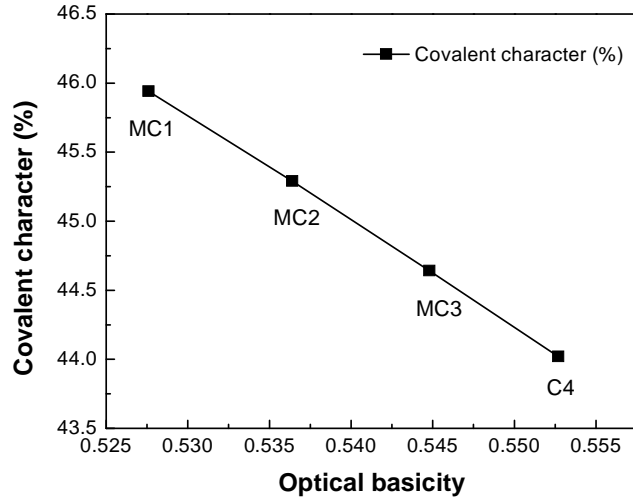


Fig. 8 - Inverse relationship of covalent character of microcomposites MC1-MC4 (for composition see Table 1) as a function of their optical basicity

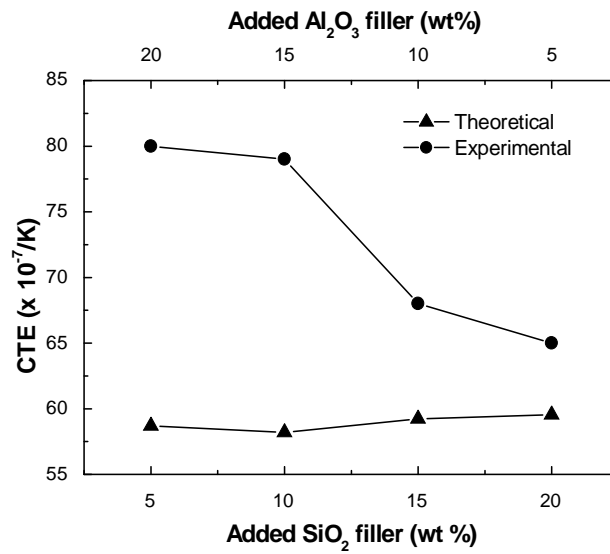


Fig. 9 - Comparison of variation of experimental and theoretically calculated coefficient of thermal expansion (CTE) as a function of added Al₂O₃ or SiO₂ filler of microcomposites MC1-MC4 (for composition see Table 1)

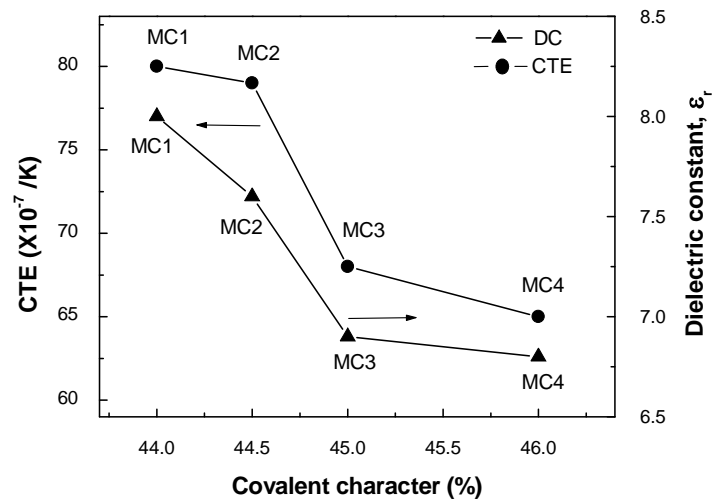


Fig. 10 - Variation of coefficient of thermal expansion (CTE) and dielectric constant (ϵ_r) of microcomposites MC1-MC4 (for composition see Table 1) as a function of their covalent character

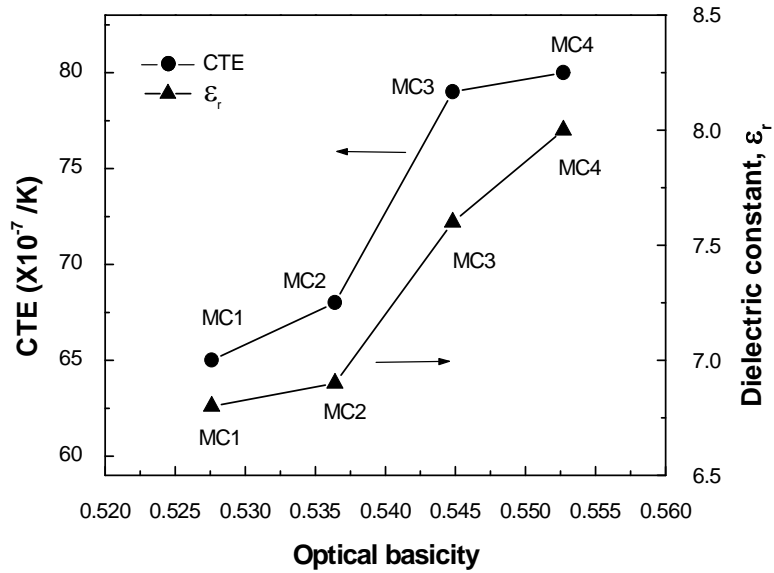


Fig. 11 - Variation of coefficient of thermal expansion (CTE) and dielectric constant (ϵ_r) of microcomposites MC1-MC4 (for composition see Table 1) as a function of their optical basicities

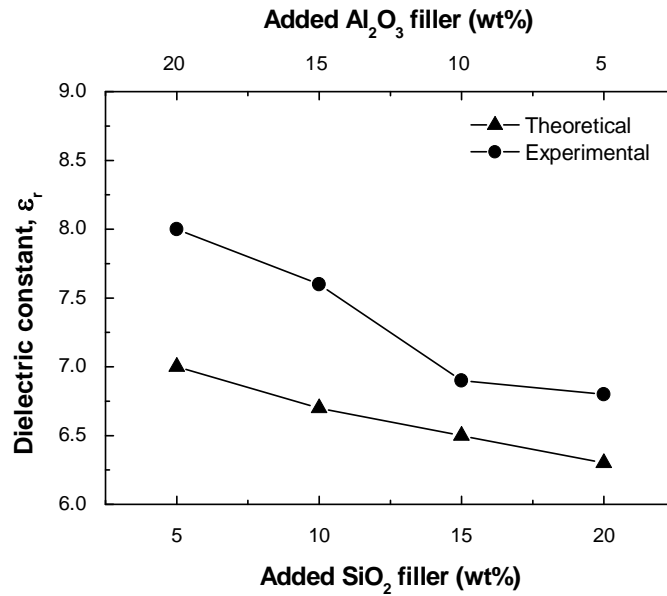


Fig. 12 - Comparison of variation of experimentally and theoretically calculated dielectric constant (ϵ_r) as a function of added Al₂O₃ or SiO₂ filler of microcomposites MC1-MC4 (for composition see Table 1)